Supporting Information for

Rational construction of a porous lanthanide coordination polymer featuring reversible guest-dependent magnetic relaxation behavior

Fang Ma,[a] Jin Xiong,[b] Yin-Shan Meng, [b] Jing Yang, [a] Hao-Ling Sun,*[a] and Song Gao*[b]

[a] *Department of Chemistry and Beijing Key Laboratory of Energy Conversion and Storage Materials, Beijing Normal University, Beijing 100875, P. R. China. E-mail: haolingsun@bnu.edu.cn;*

[b] *Beijing National Laboratory for Molecular Sciences, State Key Laboratory of Rare Earth Materials Chemistry and Applications, College of Chemistry and Molecular Engineering, Peking University, Beijing 100871, China. E-mail: gaosong@pku.edu.cn;*

Experimental Section

X-ray crystallography and physical measurement

Intensity data for crystals of **1**-**3** were collected on a rigaku SuperNova, Dual, AtlasS2 diffractometer with graphite-monochromated Mo Kα (for **1** and **2**) or Cu Kα (for **3**) radiation at 100 K. Using Olex2, the structure was solved with the olex2.solve structure solution program using Charge Flipping and refined with the olex2.refine refinement package using Gauss-Newton minimisation. All non-hydrogen atoms were refined anisotropically. Hydrogen atoms were placed at the calculation positions. The details of crystallographic data and selected bond parameters for complexes **1**, **2** and **3** are listed in Table S2 and Table S3, respectively.

Elemental analyses of carbon, hydrogen, and nitrogen were carried out with an Elementar Vario EL analyzer. FTIR spectra were recorded in the range of 4000 to 400 cm^{-1} on an AVATAR 360 Nicolet 380 FT/IR spectrometer using KBr pellets. Thermogravimetric analyses (TGA) were carried out using a Mettler-Toledo

TGA/DSC1 in N_2 or air flow, from 25 ℃ to 1000 ℃ and 25 ℃ to 350 ℃ with a heating rate of 5 ℃/min. Powder X-ray diffraction (PXRD) analyses were performed on a Rigaku Dmax-2000 X-ray diffractometer with Cu Kα (λ = 1.54059 Å) radiation. Variable-temperature magnetic susceptibility measurements of **1**, **2** and **3** were performed on Quantum Design PPMS magnetometer (100~10000 Hz) and Quantum Design SQUID-MPMS3 (1~1000 Hz) magnetometer.

Computational details

Complete-active-space self-consistent field (CASSCF) calculations on the Dy^{3+} ion fragments of complexes **1-3** on the basis of X-ray determined geometry have been carried out with *MOLCAS* 8.1 program package. For Complex **1**, the influence of neighboring Dy^{3+} ion was taken into account by diamagnetic Lu^{3+} ion. For Complex **2-3**, there is only one type of Dy^{3+} ion, and thus we only need to calculate one Dy^{3+} ion fragment. During the calculations, the other Dy^{3+} ion was replaced by diamagnetic Lu^{3+} ion, the model structure as show in Fig. S29.

For CASSCF calculations, the basis sets for all atoms are atomic natural orbitals from the MOLCAS ANO-RCC library: ANO-RCC-VTZP for Dy^{3+} ion; VTZ for close O and N; VDZ for distant atoms. The calculations employed the second order Douglas-Kroll-Hess Hamiltonian, where scalar relativistic contractions were taken into account in the basis set and the spin-orbit coupling was handled separately in the restricted active space state interaction (RASSI-SO) procedure. For the fragment of Dy^{3+} ion, the active electrons in 7 active spaces include all f electrons CAS (9, 7) for Complexes **1**-**3** in the CASSCF calculation. To exclude all the doubts we calculated all the roots in the active space. We have mixed the maximum number of spin-free state which was possible with our hardware (all from 21 sextets, 128 from 224 quadruplets and 130 from 490 doublets for Dy^{3+} ion fragments).

Fitting the exchange interaction in two complexes using Lines model based on CASSCF results

To fit the exchange interaction in Complex **2-3**, we took two steps to obtain them. Firstly, we calculated one Dy^{3+} ion fragment using CASSCF to obtain the

corresponding magnetic properties. Then, the exchange interaction between the magnetic centers is considered within the Lines model, while the account of the dipole-dipole magnetic coupling is treated exactly. The Lines model is effective and has been successfully used widely in the research field of f-element single-molecule magnets.

For compounds **2**-**3**, there is only one type of *J*.

The exchange Hamiltonian is:

$$\widehat{H}_{exch} = -J_{total}\,\hat{\tilde{S}}_{Dy1}\,\hat{\tilde{S}}_{Dy1A} \qquad \text{(S1)}$$

The J_{total} is the parameter of the total magnetic interaction ($J_{total} = J_{diploar} + J_{exchange}$) between magnetic center ions. The $\hat{S}_{Dy} = \pm 1/2$ are the ground pseudospin on the Dy^{3+} ion sites. The dipolar magnetic coupling can be calculated exactly, while the exchange coupling constant was fitted through comparison of the computed and measured magnetic susceptibility and molar magnetization using the POLY_ANISO program.

Table S1. Some typical examples of lanthanide coordination polymers featuring slow magnetic relaxation.

Structural formula	Dimension	Magnetic interaction	DC field (Oe)	*U*eff (K)	Ref
$[Dy(NTC)_2(phen)(m_2\text{-}OH)(m_2\text{-}H_2O)]n$	1	ferromagnetic	0	567	7d
$[Cp^*_2DyCl_2K(THF)]_n$	1	antiferromagnetic	0	545	4v
$[\{Dy(L)\ (\mu_2\text{-bpdo})_{0.5}(\mu_4\text{-bpdo})_{0.5}\ (CH_3OH)\}\cdot ClO_4\cdot 3CH_3OH]_n$	3	antiferromagnetic	0	393	This work
$\{[Dy(3\text{-}OHpy)_2(H_2O)_4][Co(CN)_6]\}\cdot H_2O$	1	antiferromagnetic	0	385	7f
$[Dy_3(Iba)_8(btaH)_2(ClO_4)(H_2O)_5]_n$	1	antiferromagnetic	0	357	4t
$[Dy(L)(H_2O)_4]Cl_2\cdot 2H_2O$	1	antiferromagnetic	0	227	8a
$[Dy(3\text{-py-4 pmc})(C_2O_4)_{0.5}(OH)(H_2O)]$	2	ferromagnetic	0	186	4d
$[DyL(HCOO)(CH_3OH)]n$	1	ferromagnetic	0	176	4u
$[Dy(phen)(L)]_n$	3	ferromagnetic	0	131	4j
$[Dy_2(dga)_2(\mu_3\text{-}OH)_2(H_2O)]\cdot H_2O$	2	ferromagnetic	0	112	4i
$Dy_2(INO)_4(NO_3)_2\cdot 2CH_3CN$	3	ferromagnetic	0	110	5c
$[Dy_2(apca)_4(\mu_2\text{-}OH)_2(H_2O)_2]_n$	2	ferromagnetic	0	59	4h
$[Dy(pno)(CH_3COO)]\cdot 0.5DMF\cdot H_2O\cdot 2CH_3OH$	2	antiferromagnetic	0	33.6	5d
$(H_3O)[Ln(NA)_2]\cdot H_2O$	2	antiferromagnetic	1000	75	4p
$\{[Dy_2(FDA)_3(DMF)_2]\cdot 1.5DMF\}_n$ $[Dy_2(FDA)_3(DMF)_2(CH3OH)]_n$	3	ferromagnetic	2000	41.8/67.5	4m
Dy(BTC)	3	antiferromagnetic	1000	45.9	5a
$(EMIM)[Dy_3(BDC)_5$	3	antiferromagnetic	2000	39.3	5q
$[Dy_2(1H\text{-}5\text{-}Cl\text{-}6\text{-}Opy\text{-}CO_2)_2(C_2O_4)_2(H_2O)]\cdot 2H_2O$	3	antiferromagnetic	2000	37.6	5r
$Dy(C_2O_4)_{1.5}phen]\cdot 0.5H_2O$	3	ferromagnetic	1200	35.5 32.6	4k
$[Ln(bipyNO)_4](TfO)_3\cdot xsolvent$	3	antiferromagnetic	1000	17.9	4g
$[Ln(hfac)_3]_2(4,4'\text{-BipyNO})_2$	3	antiferromagnetic	1900	10.3	4l

Abbreviations: NTC = 4-nitrobenzoic acid, phen=1,10-phenanthroline; Cp = cyclopentadiene; 3-OHpy = 3-hydroxypyridine; 3-py-4-pmc = 2-(3-pyridyl)pyrimidine-4-carboxylate; IbaH = isobutyric acid, btaH = benzotriazole; L = N'-(2-hydroxybenzylidene) pyridine-N-oxide-carbohydrazide; 3-py-4 pmc = 2-(3-pyridyl) pyrimidine-4-carboxylic acid; L = N′-(2-hydroxybenzylidene)picolinohydrazide; phen= 1, 10-phenanthroline, L= 5-hydroxyisophthalic acid; dga=2,2-dimethylglutaric acid(H_2L); HINO = nicotinic acid N-oxide; Hapca: 3-aminopyrazine-2-carboxylic acid; pno = N′-(2-hydroxy-3-methoxybenzylidene)pyridine-N-oxide carbohydrazide; H_2NA = 5-hydroxynicotinic acid; H_2FDA = furan-2,5-dicarboxylic acid; BTC =1,3,5-benzenetricarboxylate; H_2BDC =1,4-benzenedicarboxylic acid，EMIM = 1-ethyl-3-methylimidazolium; 1H-5-Cl-6-Opy-3-CO_2 = 1-hydro-5-chloro-6-oxopyridine-3-carboxylate; bipyNO = 4,4'-bipyridine-N,N'-dioxide, TfO = triflate; (hfac = hexafluoro-acetylacetonate, 4,4'-BipyNO = 4,4′-bipyridine N,N'-dioxide;

Table S2. Crystallographic data and Structure Refinement for complexes **1**, **2** and **3**.

Formula	$C_{16}H_{26}DyN_3O_8Cl_2$	$C_{27}H_{34}DyN_5O_{13}Cl$	$C_{24}H_{22}DyN_5O_{10}Cl$
Mr	621.80	834.54	738.41
Crystal system	monoclinic	triclinic	triclinic
Space group	$P\ 2_1/n$	$P\ \bar{1}$	$P\ \bar{1}$
T(K)	100 K	100 K	100 K
a(Å)	8.5612(3)	11.8598(6)	11.0697(15)
b(Å)	15.4837(5)	12.0997(7)	11.7807(16)
c(Å)	17.4652(6)	13.4297(7)	12.2202(17)
a(°)	90	102.794(5)	62.152(14)
β(°)	94.758(3)	98.239(4)	71.245(12)
γ(°)	90	117.449(5)	81.049(11)
V (Å^3)	2307.17(12)	1599.30(15)	1334.2(3)
Z	4	2	2
μ (mm^{-1})	3.515	2.492	16.492
F(000)	1228	836	728
GOF	1.034	1.030	1.089
Data collected	12761	11065	7893
Unique	4874	6717	4734
R_{int}	0.0531	0.0585	0.0297
$R1$,$wR2$[$I>2\sigma(I)$]	0.0379, 0.0675	0.0543, 0.0986	0.1014, 0.2851
R1, wR2 [all data]	0.0555, 0.0762	0.0703, 0.1089	0.1141, 0.3087

Table S3. Selected Bond Distances (Å) in complexes **1**, **2** and **3.**

	1		**2**	**3**
Dy-O1	2.154(3)	Dy-O1	2.189(4)	2.150(17)
Dy-O2	2.420(3)	Dy-O2	2.321(4)	2.328(8)
Dy-O3 #1	2.340(3)	Dy-O3 #1	2.370(4)	2.343(12)
Dy-O4	2.338(4)	Dy-O4	2.406(4)	2.422(10)
Dy-O5	2.370(3)	Dy-O4#2	2.466(4)	2.458(8)
Dy-O6	2.387(3)	Dy-O5	2.316(4)	2.306(11)
Dy-O7	2.462(3)	Dy-O6	2.421(4)	2.445(15)
Dy-N1	2.536(4)	Dy-N1	2.496(5)	2.492(10)

Table S4. Hydrogen Bonds in **1**.

D-H	d(D-H) (Å)	<DHA(°)	d(D…A) (Å)	A
N2-H13	0.762	129.77	2.642	O1(x, y, z)
O10-H10A	0.930	164.85	2.688	O11(x,y,z+1)

Table S5. Hydrogen Bonds in **2**.

D-H	d(D-H) (Å)	<DHA(°)	d(D…A) (Å)	A
O7-H7a	0.803	166.36	2.000	N2(1-x,1-y,1-z)
O6-H6	0.859	157.32	1.842	O8(x, y, z)

Table S6. Relaxation fitting parameters from Least-Squares Fitting of $\chi(f)$ data under zero dc field of **1**.

T/K	χ_T	χ_s	α	τ
2	7.52	0.54	0.18	0.029
2.5	6.12	0.40	0.19	0.028
3	5.12	0.34	0.18	0.028
3.5	4.43	0.27	0.19	0.027
4	3.92	0.20	0.23	0.027
4.5	3.32	0.20	0.21	0.026
5	3.09	0.16	0.22	0.025
5.5	2.86	0.14	0.22	0.024
6	2.62	0.12	0.22	0.022
6.5	2.41	0.11	0.21	0.020
7	2.23	0.11	0.19	0.018
7.5	2.08	0.085	0.18	0.015
8	1.94	0.068	0.17	0.013
8.5	1.81	0.067	0.14	0.011
9	1.71	0.044	0.14	0.0086
9.5	1.61	0.042	0.13	0.0070
10	1.52	0.040	0.11	0.0057
10.5	1.45	0.039	0.094	0.0047
11	1.38	0.037	0.085	0.0038
11.5	1.32	0.035	0.074	0.0032
12	1.26	0.034	0.066	0.0026
12.5	1.21	0.032	0.062	0.0022
13	1.17	0.031	0.059	0.0018
13.5	1.12	0.032	0.052	0.0016
14	1.08	0.033	0.047	0.0013
14.5	1.04	0.032	0.044	0.0011
15	1.01	0.032	0.042	9.66E-4
15.5	0.98	0.029	0.067	8.18E-4
16	0.95	0.017	0.082	6.25E-4
16.5	0.92	0.017	0.086	5.22E-4
17	0.90	0.017	0.092	4.44E-4
17.5	0.86	0.018	0.084	3.72E-4
18	0.83	0.020	0.074	3.10E-4
18.5	0.81	0.020	0.088	2.56E-4
19	0.78	0.024	0.078	2.09E-4
19.5	0.78	0.019	0.11	1.70E-4
20	0.75	0.023	0.11	1.35E-4
20.5	0.73	0.027	0.11	1.07E-4
21	0.71	0.030	0.11	8.31E-5

21.5	0.70	0.035	0.11	6.49E-5
22	0.68	0.037	0.12	5.01E-5
22.5	0.66	0.043	0.11	3.87E-5
23	0.65	0.044	0.12	2.96E-5
23.5	0.64	0.045	0.12	2.25E-5
24	0.62	0.048	0.13	1.72E-5
24.5	0.61	0.059	0.13	1.35E-5

Table S7. Relaxation fitting parameters from Least-Squares Fitting of χ(f) data under 2 kOe dc field of **1**.

T/K	χT	χs	α	τ
8	1.72	0.013	0.051	0.069
8.5	1.65	0.013	0.058	0.046
9	1.55	0.013	0.044	0.031
9.5	1.47	0.012	0.042	0.021
10	1.41	0.012	0.041	0.015
10.5	1.33	0.012	0.042	0.011
11	1.28	0.012	0.042	0.0084
11.5	1.23	0.011	0.043	0.0063
12	1.17	0.011	0.034	0.0050
12.5	1.12	0.010	0.042	0.0039
13	1.09	0.010	0.041	0.0031
13.5	1.04	0.012	0.026	0.0026
14	1.01	0.0090	0.040	0.0021
14.5	0.98	0.0064	0.051	0.0017
15	0.93	0.019	0.054	0.0015
15.5	0.91	0.015	0.027	0.0012
16	0.89	0.014	0.054	9.30E-4
16.5	0.87	0.013	0.013	7.72E-4
17	0.83	0.016	0.052	6.30E-4
17.5	0.81	0.017	0.056	5.19E-4
18	0.85	0.012	0.12	4.33E-4
18.5	0.83	0.013	0.12	3.45E-4
19	0.80	0.014	0.13	2.72E-4
19.5	0.78	0.016	0.13	2.11E-4
20	0.76	0.019	0.14	1.63E-4
20.5	0.74	0.022	0.14	1.24E-4
21	0.72	0.025	0.14	9.40E-5
21.5	0.71	0.028	0.14	7.10E-5
22	0.69	0.032	0.14	5.36E-5
22.5	0.67	0.035	0.14	4.02E-5
23	0.66	0.025	0.16	2.91E-5
23.5	0.64	0.039	0.15	2.26E-5
24	0.63	0.018	0.17	1.58E-5
24.5	0.62	0.022	0.17	1.20E-5

Table S8. Relaxation fitting parameters from Least-Squares Fitting of $\chi(f)$ data under zero dc field of **2**.

T/K	χ_T	χ_s	α	τ
7	1.70	0.061	0.098	0.098
7.5	0.12	0.063	0.10	0.088
8	1.65	0.048	0.14	0.066
8.5	1.54	0.048	0.13	0.046
9	1.46	0.047	0.13	0.033
9.5	1.38	0.046	0.12	0.025
10	1.32	0.045	0.12	0.019
10.5	1.26	0.044	0.11	0.014
11	1.21	0.044	0.10	0.011
11.5	1.15	0.044	0.096	0.0088
12	1.11	0.043	0.097	0.0071
12.5	1.07	0.042	0.098	0.0057
13	1.03	0.042	0.090	0.0047
13.5	0.99	0.040	0.093	0.0038
14	0.96	0.040	0.089	0.0032
14.5	0.93	0.042	0.083	0.0027
15	0.90	0.041	0.087	0.0023
15.5	0.87	0.042	0.080	0.0019
16	0.84	0.047	0.066	0.0016
16.5	0.82	0.040	0.088	0.0014
17	0.80	0.044	0.079	0.0012
17.5	0.78	0.049	0.068	0.0010
18	0.76	0.049	0.075	9.02E-4
18.5	0.74	0.053	0.069	7.86E-4
19	0.72	0.052	0.071	6.87E-4
19.5	0.70	0.056	0.072	6.03E-4
20	0.68	0.064	0.060	5.31E-4
20.5	0.67	0.066	0.064	4.65E-4
21	0.66	0.063	0.074	4.05E-4
21.5	0.64	0.070	0.070	3.58E-4
22	0.63	0.030	0.083	2.92E-4
22.5	0.61	0.031	0.080	2.52E-4
23	0.60	0.031	0.088	2.18E-4
23.5	0.59	0.032	0.084	1.89E-4
24	0.58	0.031	0.095	1.62E-4
24.5	0.57	0.033	0.094	1.40E-4
25	0.56	0.032	0.099	1.19E-4
25.5	0.55	0.032	0.10	1.02E-4
26	0.54	0.032	0.11	8.64E-5

26.5	0.53	0.034	0.11	7.34E-5
27	0.52	0.030	0.12	6.11E-5
27.5	0.51	0.034	0.11	5.19E-5
28	0.50	0.033	0.12	4.36E-5
28.5	0.49	0.041	0.10	3.74E-5
29	0.48	0.035	0.11	3.07E-5
29.5	0.47	0.029	0.13	2.50E-5
30	0.46	0.050	0.096	2.26E-5
30.5	0.45	0.049	0.098	1.88E-5
31	0.45	0.043	0.11	1.52E-5
31.5	0.44	0.091	0.044	1.61E-5
32	0.43	0.075	0.073	1.21E-5

Table S9. Relaxation fitting parameters from Least-Squares Fitting of $\chi(f)$ data under zero dc field of **3**.

T/K	χ_T	χ_s	α	τ
7	2.04	0.074	0.27	0.22
7.5	1.91	0.055	0.29	0.14
8	1.59	0.079	0.21	0.075
8.5	1.49	0.071	0.21	0.051
9	1.39	0.079	0.18	0.036
9.5	1.33	0.074	0.18	0.027
10	1.26	0.076	0.18	0.020
10.5	1.21	0.064	0.19	0.015
11	1.16	0.064	0.19	0.012
11.5	1.11	0.067	0.17	0.0091
12	1.06	0.068	0.16	0.0072
12.5	1.03	0.068	0.16	0.0057
13	0.99	0.069	0.16	0.0046
13.5	0.96	0.069	0.15	0.0038
14	0.90	0.070	0.14	0.0030
14.5	0.89	0.072	0.14	0.0025
15	0.86	0.068	0.15	0.0021
15.5	0.84	0.070	0.15	0.0017
16	0.81	0.073	0.14	0.0015
16.5	0.79	0.071	0.15	0.0012
17	0.77	0.068	0.16	0.0010
17.5	0.75	0.074	0.15	8.50E-4
18	0.73	0.074	0.15	7.13E-4
18.5	0.70	0.086	0.14	6.11E-4
19	0.68	0.10	0.10	5.35E-4
19.5	0.68	0.069	0.18	4.18E-4
20	0.64	0.034	0.20	3.97E-4
20.5	0.63	0.032	0.22	3.31E-4
21	0.63	0.029	0.24	2.82E-4
21.5	0.61	0.027	0.25	2.28E-4
22	0.59	0.028	0.24	1.86E-4
22.5	0.58	0.024	0.26	1.53E-4
23	0.57	0.024	0.26	1.24E-4
23.5	0.55	0.025	0.27	1.03E-4
24	0.54	0.023	0.28	8.32E-5
24.5	0.53	0.027	0.27	6.82E-5
25	0.52	0.027	0.28	5.52E-5
25.5	0.51	0.029	0.28	4.55E-5
26	0.50	0.036	0.27	3.81E-5

26.5	0.48	0.045	0.26	3.30E-5
27	0.47	0.060	0.23	2.90E-5
27.5	0.46	0.046	0.26	2.19E-5
28	0.45	0.077	0.21	2.12E-5

Table S10. Calculated energy levels (cm^{-1}) and ***g*** (g_x, g_y, g_z) tensors of the lowest Kramers doublets (KDs) of the Dy fragments of complexes **1-3**.

KDs	**1（dy_1d）**		**2(dy_3d)**		**3(dy_3d)**	
	E	***g***	*E*	***g***	*E*	***g***
1	0.0	0.002 0.003 19.609	0.0	0.002 0.003 19.645	0.0	0.001 0.002 19.757
2	198.7	0.567 1.976 13.648	174.6	0.070 0.086 16.622	253.8	0.024 0.029 16.988
3	228.2	1.017 1.129 13.336	295.3	0.788 0.929 15.468	462.7	0.022 0.128 13.858
4	332.5	4.149 5.011 11.872	330.4	1.606 4.699 11.219	551.1	2.038 6.386 12.706
5	371.8	1.276 5.350 10.548	373.2	2.165 4.026 8.756	586.7	2.554 5.133 8.960
6	423.6	1.338 2.996 14.439	430.8	1.871 3.365 7.344	634.2	2.368 5.217 9.093
7	480.4	0.159 1.376 17.417	470.2	2.054 6.666 12.501	679.5	2.522 3.961 11.410
8	519.4	0.353 1.033 18.648	534.8	0.129 0.281 19.068	760.6	0.043 0.422 17.996

Table S11. Wavefunction composition for the eight Kramer doublets of the $^6H_{15/2}$ ground multiplet of complexes **1-3**.

KDs	**1（dy_1d）**
1	0.96|±15/2⟩
2	0.58|±13/2⟩+0.09|±5/2⟩+0.09|±3/2⟩+0.12|±1/2⟩
3	0.30|±13/2⟩+0.07|±5/2⟩+0.23|±3/2⟩+0.30|±1/2⟩
4	0.27|±11/2⟩+0.19|±7/2⟩+0.12|±5/2⟩+0.12|±3/2⟩+0.23|±1/2⟩
5	0.37|±11/2⟩+0.26|±5/2⟩+0.17|±3/2⟩
6	0.12|±11/2⟩+0.26|±9/2⟩+0.10|±7/2⟩+0.21|±3/2⟩+0.20|±1/2⟩
7	0.25|±9/2⟩+0.23|±7/2⟩+0.10|±7/2⟩+0.26|±5/2⟩+0.10|±3/2⟩
8	0.13|±11/2⟩+0.26|±9/2⟩+0.32|±7/2⟩+0.14|±5/2⟩+0.10|±3/2⟩
KDs	**2(dy_3d)**
1	0.96|±15/2⟩
2	0.91|±13/2⟩+0.07|±9/2⟩
3	0.45|±11/2⟩+0.26|±7/2⟩+0.11|±5/2⟩
4	0.23|±11/2⟩+0.23|±5/2⟩+0.32|±3/2⟩+0.16|±1/2⟩
5	0.15|±11/2⟩+0.14|±9/2⟩+0.48|±1/2⟩
6	0.43|±9/2⟩+0.11|±7/2⟩+0.24|±3/2⟩+0.21|±3/2⟩+0.10|±1/2⟩
7	0.29|±7/2⟩+0.24|±5/2⟩+0.19|±3/2⟩+0.16|±1/2⟩
8	0.09|±11/2⟩+0.17|±9/2⟩+0.27|±7/2⟩+0.27|±5/2⟩+0.12|±3/2⟩
KDs	**3(dy_3d)**
1	0.98|±15/2⟩
2	0.94|±13/2⟩
3	0.87|±11/2⟩+0.06|±7/2⟩
4	0.22|±9/2⟩+0.10|±7/2⟩+0.31|±5/2⟩+0.25|±3/2⟩
5	0.36|±9/2⟩+0.10|±7/2⟩+0.18|±3/2⟩+0.31|±1/2⟩
6	0.37|±9/2⟩+0.20|±7/2⟩+0.19|±5/2⟩+0.09|±3/2⟩+0.11|±1/2⟩
7	0.44|±7/2⟩+0.14|±5/2⟩+0.16|±3/2⟩+0.22|±1/2⟩
8	0.10|±7/2⟩+0.35|±5/2⟩+0.33|±3/2⟩+0.22|±1/2⟩

Table S12. Fitted exchange coupling constant J_{exch}, the calculated dipole-dipole interaction $J_{dipolar}$ and the total J between Dy^{3+} ions in **2** and **3** (cm^{-1}).

		2	**3**
J	$J_{dipolar}$	-2.18	-2.14
	J_{exch}	-0.5	-0.25
	J_{total}	-2.68	-2.39

Table S13. The *CShM* values calculated by *SHAPE 2.0* for **2** and **3**.

Coordination Geometry	**2**	Coordination Geometry	**3**
Snub diphenoid J84(D_{2d})	2.496	Johnson elongated triangular bipyramid J14 (D_{3h})	2.685
Biaugmented trigonal prism(C_{2v})	2.384	Snub diphenoid J84 (D_{2d})	2.383
Triangular dodecahedron(D_{2d})	0.865	Triangular dodecahedron(D_{2d})	1.205

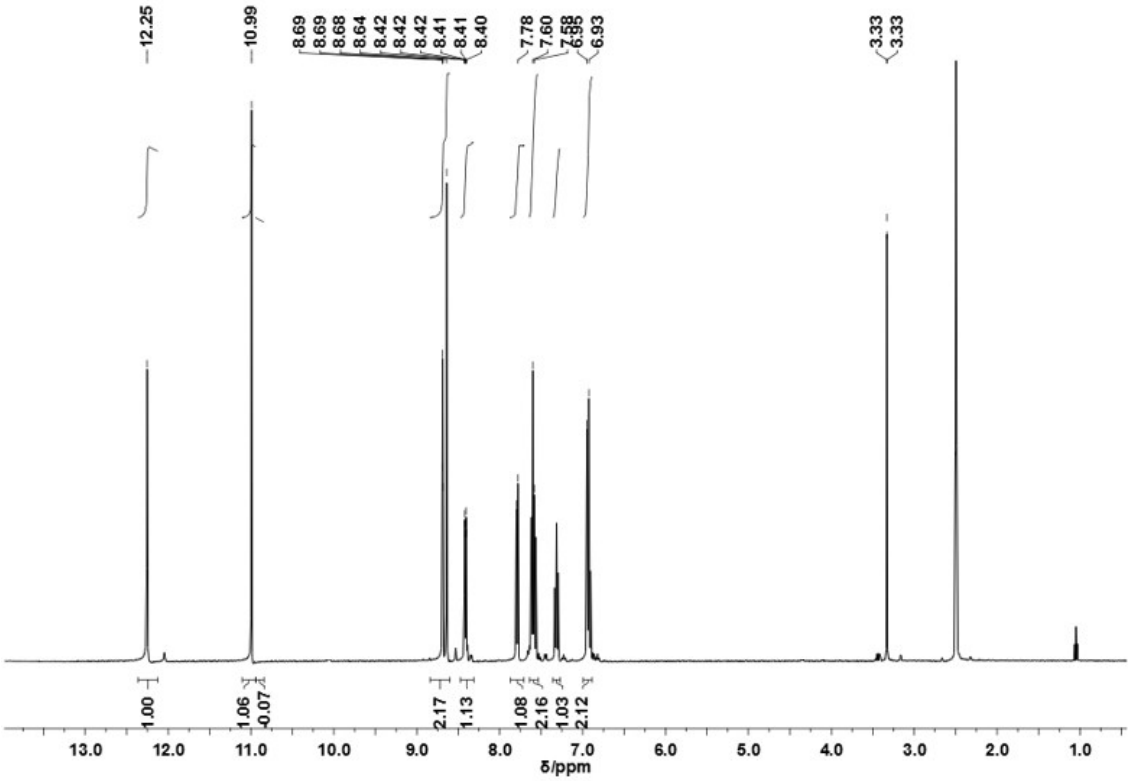

Fig S1. ^{1}HNMR spectra of H_2L.

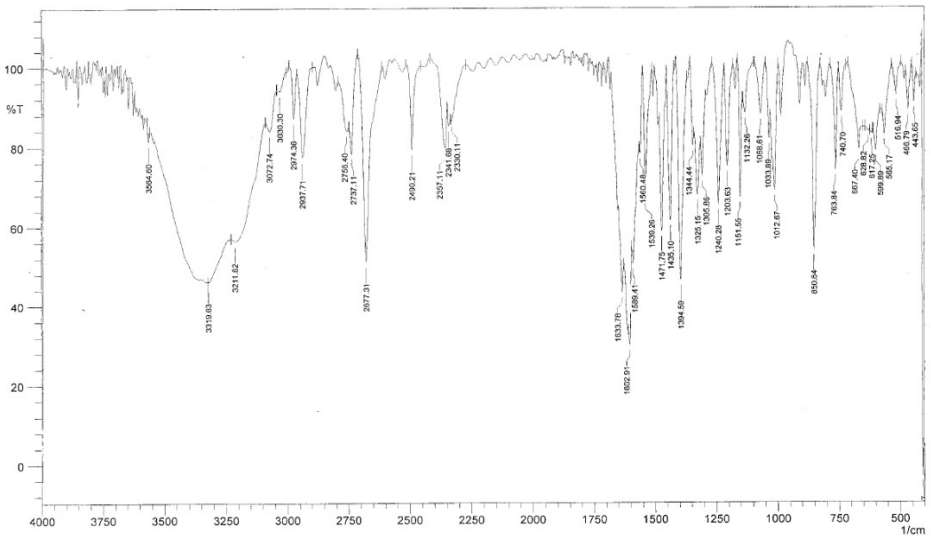

(a)

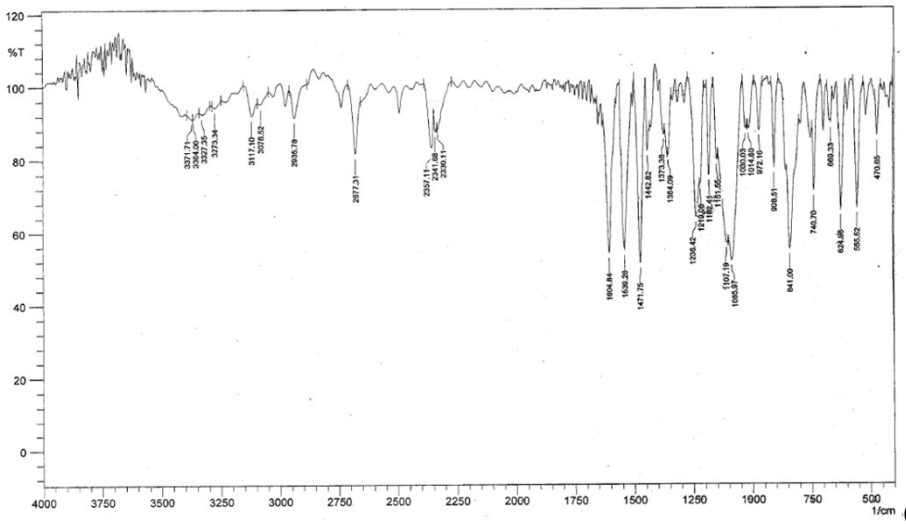

(b)

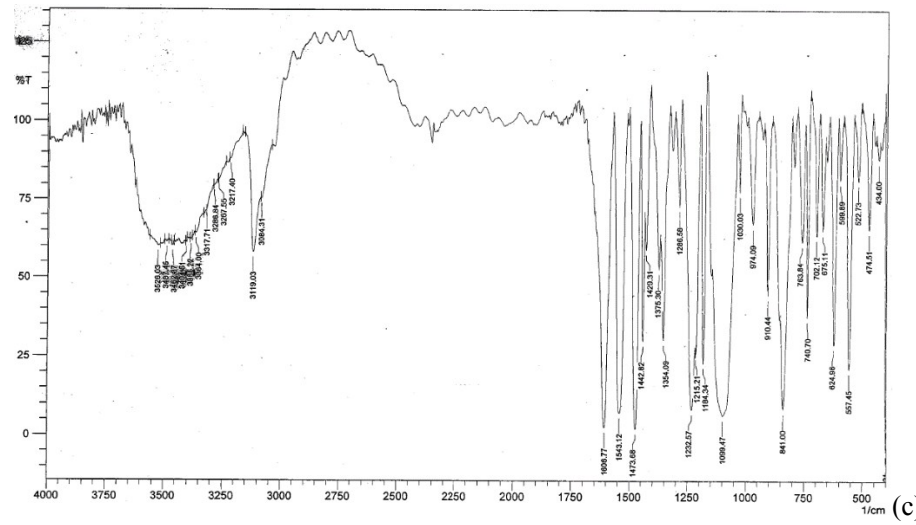

(c)

Fig S2. IR spectra for 1 (a) 2 (b) and 3 (c).

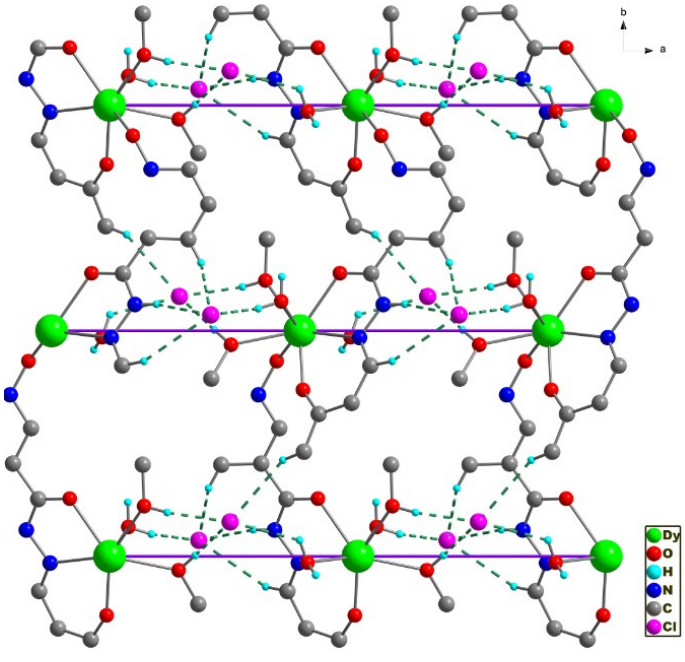

(a)

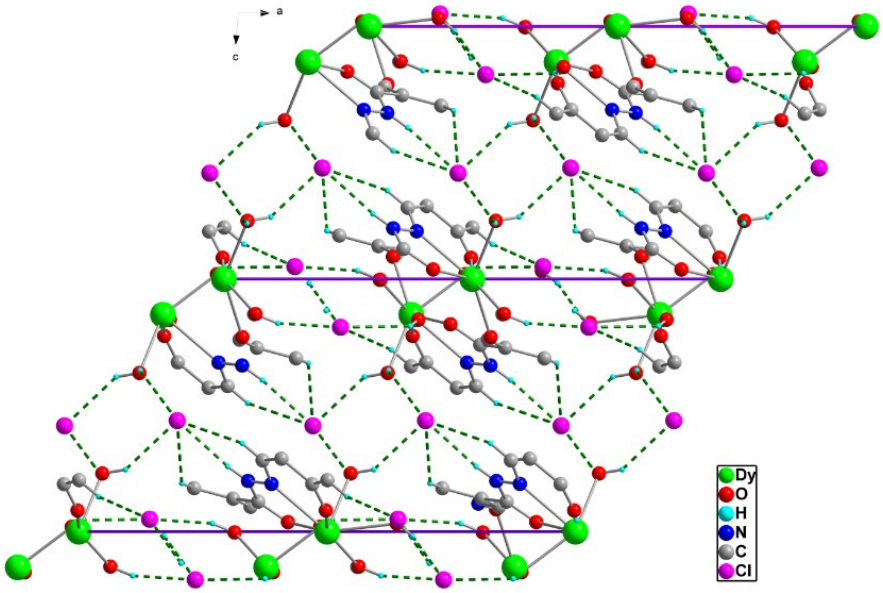

(b)

Fig S3. 2D supramolecular plane of **1** connected by hydrogen bonds (a) and 3D supramolecular structure constructed by numerous hydrogen bonds.(b).

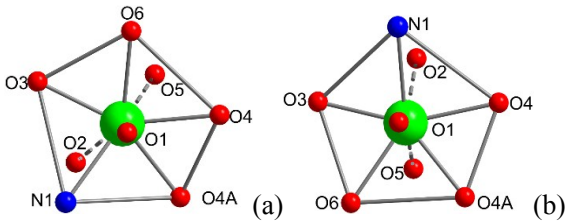

Fig S4. Coordination polyhedron around Dy^{3+} ion of **2**(a) and **3**(b).

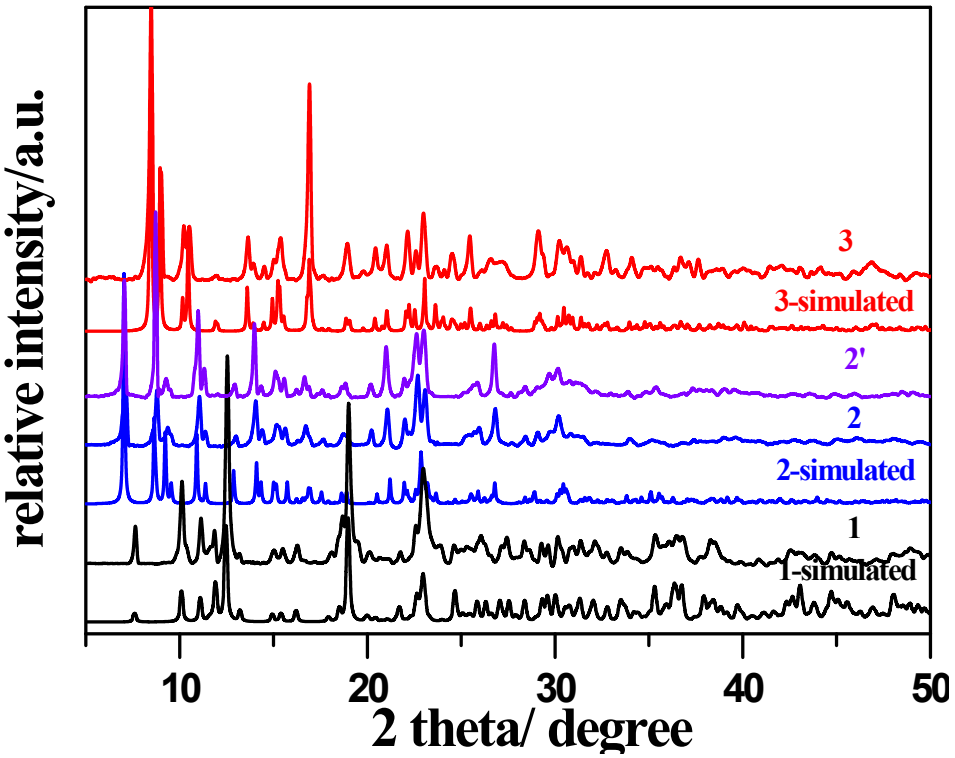

Fig. S5 Powder X-ray diffraction profiles of **1**, **2**, **3** and **2'** together with a simulation from the single crystal data.

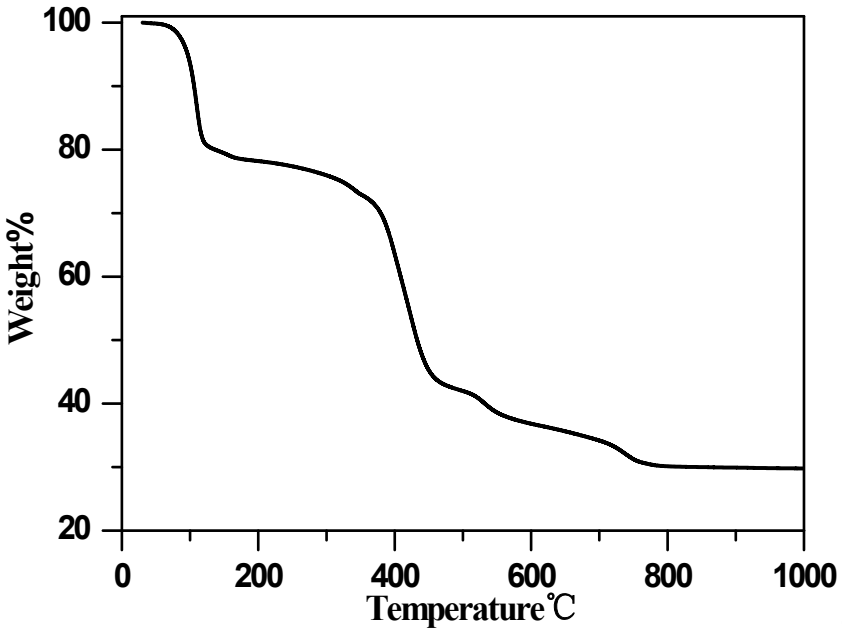

(a)

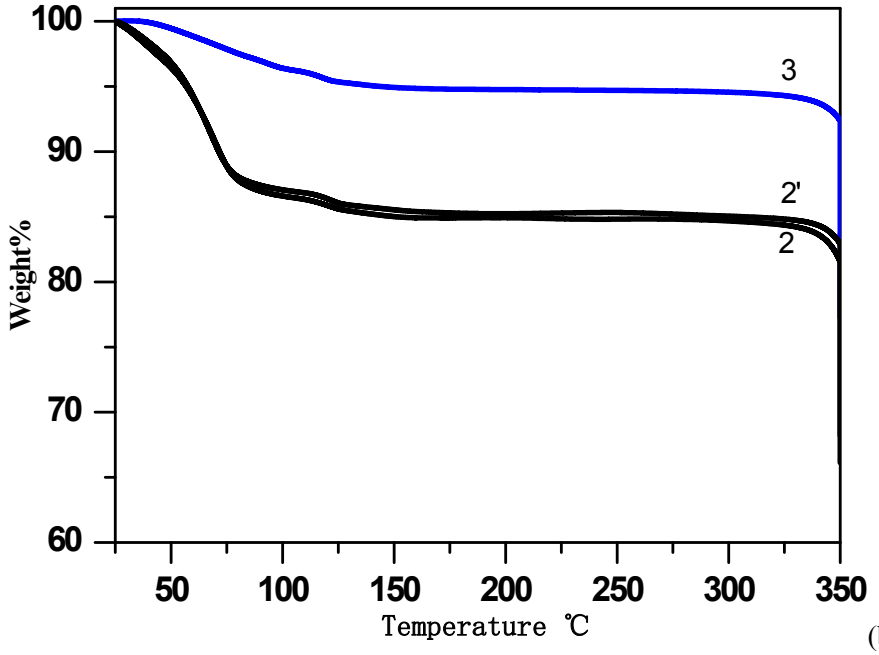

(b)

Fig. S6 TGA curves of complex **1**(a) and **2**, **3**, **2'** (b).

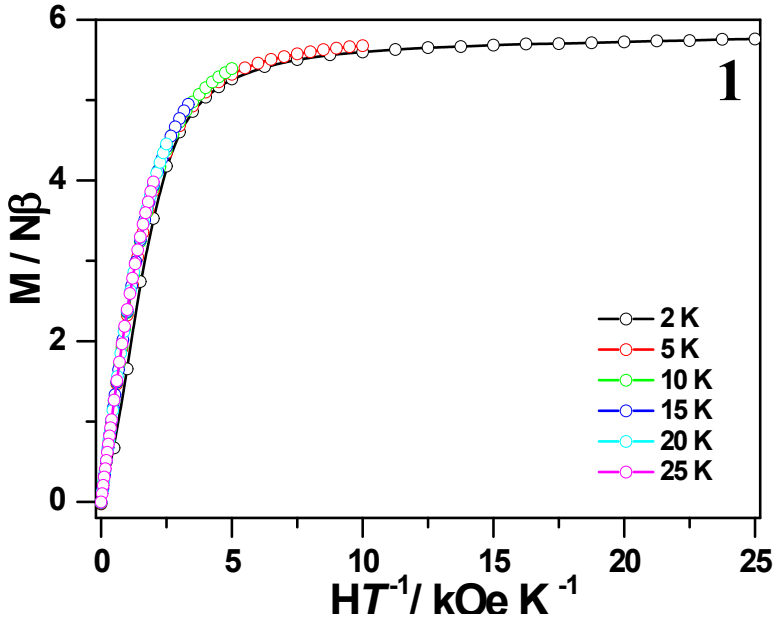

Fig. S7 Plots of *M*-*H* for **1**.

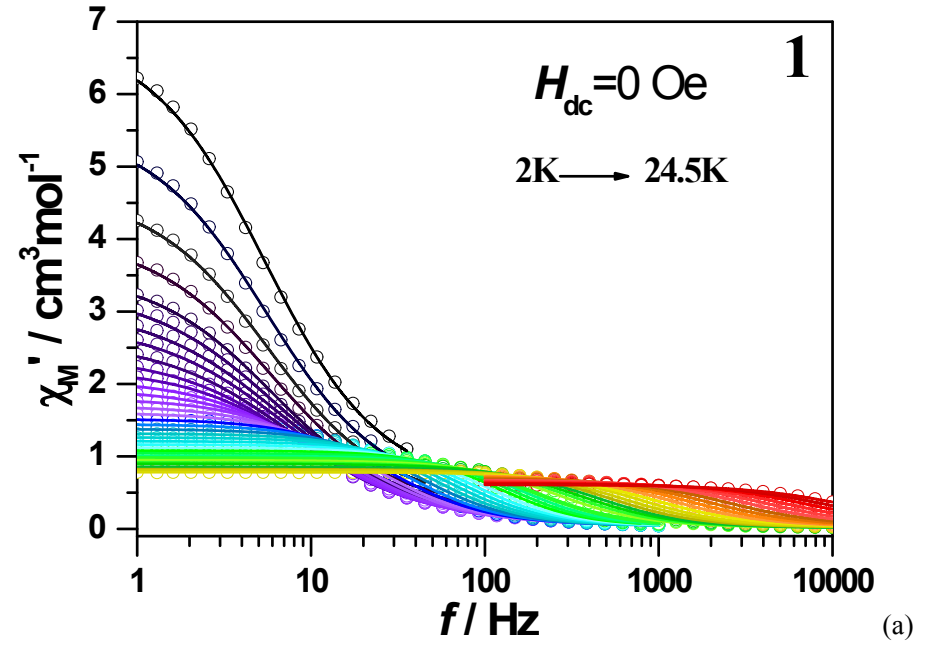

(a)

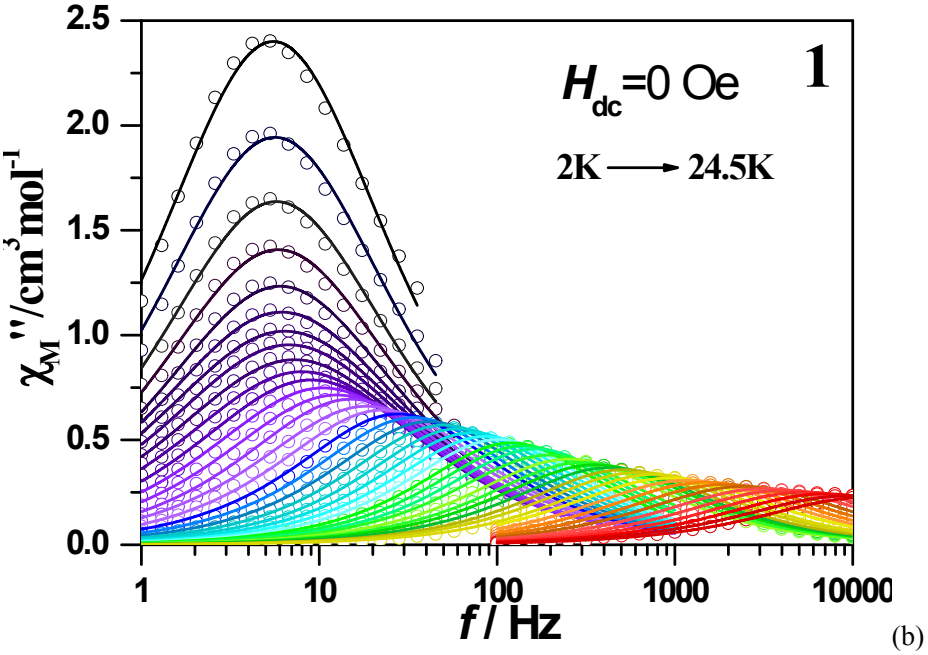

(b)

Fig. S8 *Ac-f* curves measured under zero *dc* fields for **1**. Solid lines were fitted using a generalized Debye relaxation model, simultaneously to χ'(*f*) and χ" (*f*) curves.

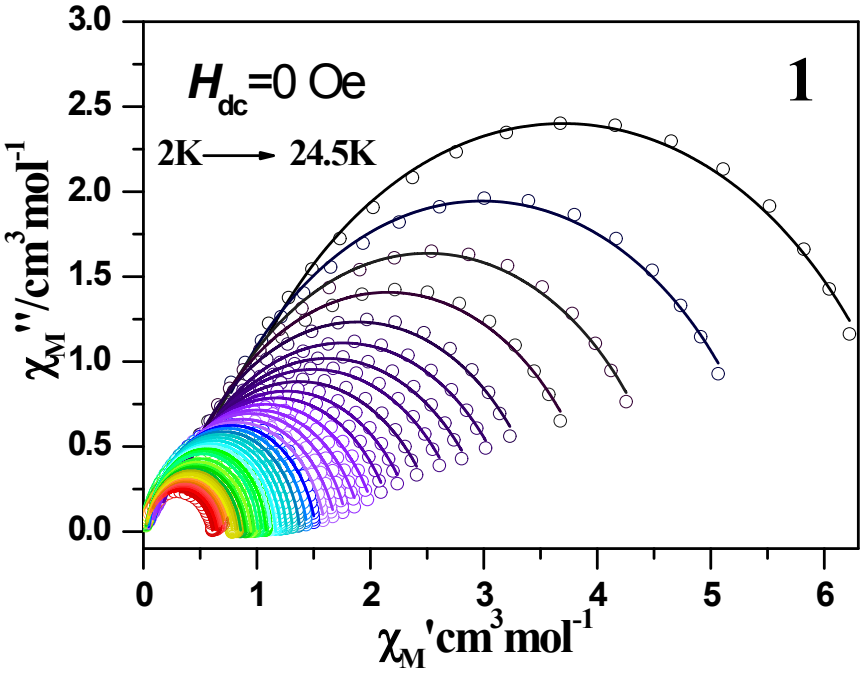

Fig. S9 Cole-cole plots of **1** under zero *dc* field.

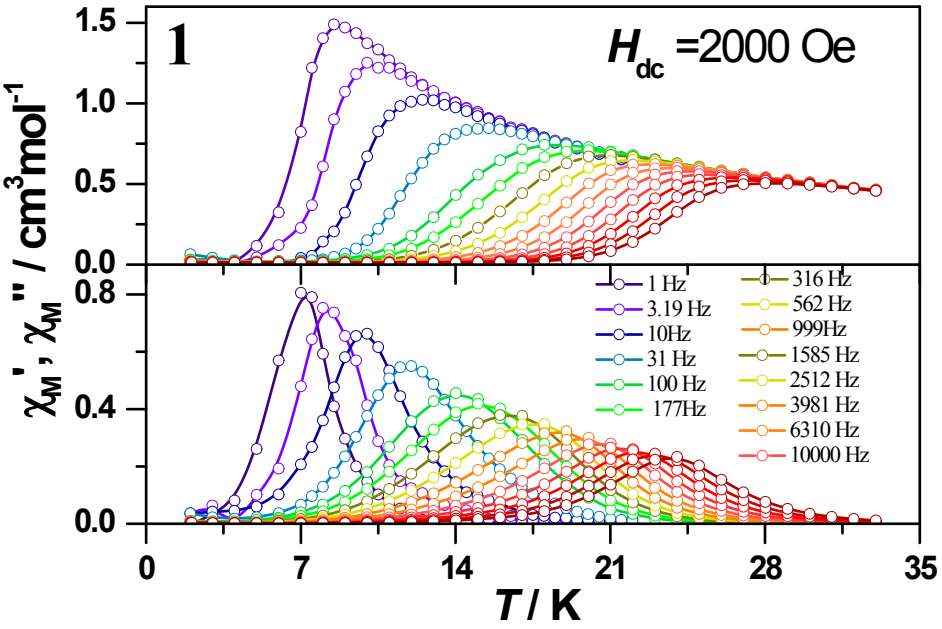

Fig. S10 The temperature dependence of ac susceptibility under 2 kOe field for **1**.

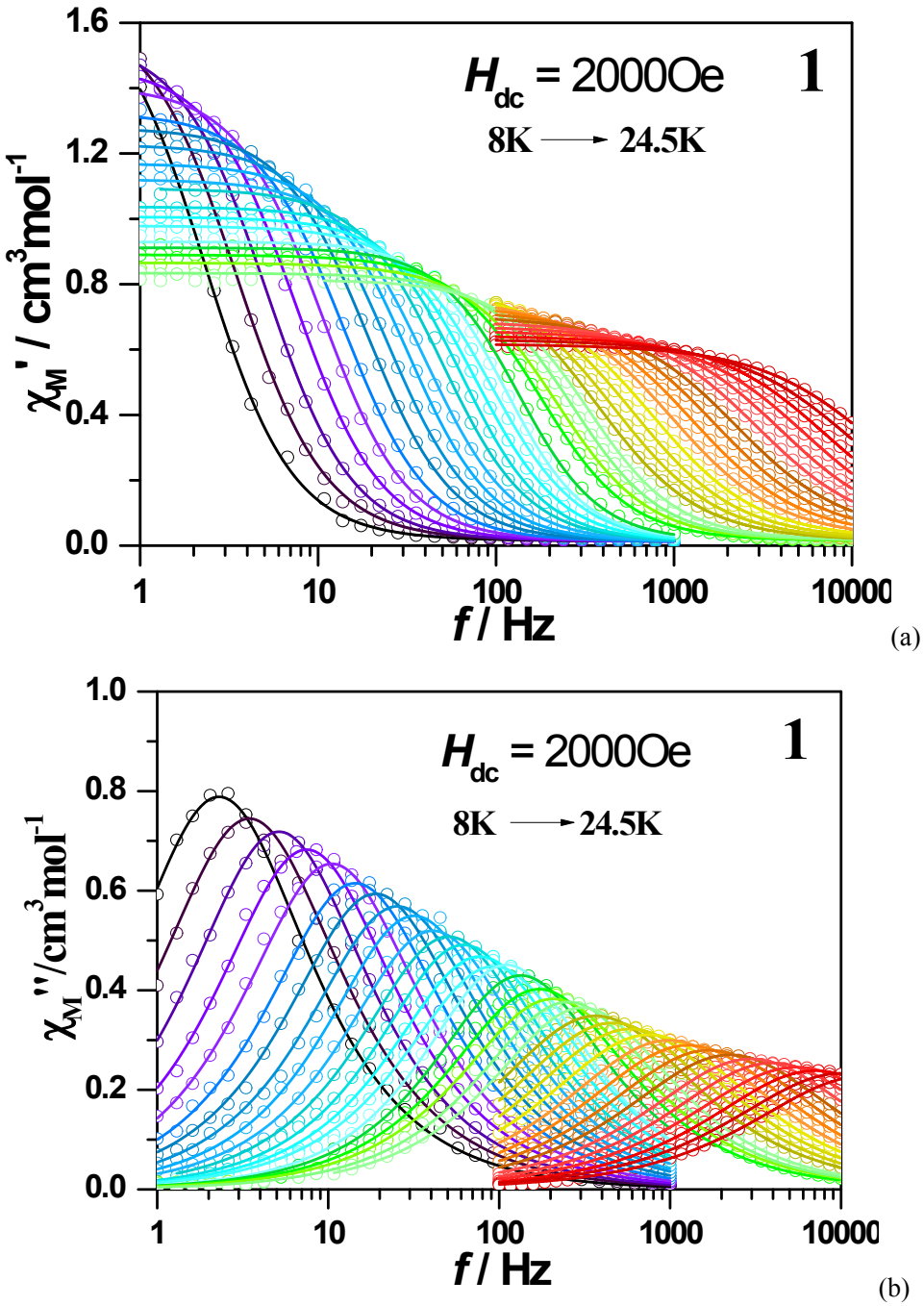

Fig. S11 *Ac-f* curves measured under 2 kOe *dc* fields for **1**. Solid lines were fitted using a generalized Debye relaxation model, simultaneously to χ'(*f*) and χ'' (*f*) curves.

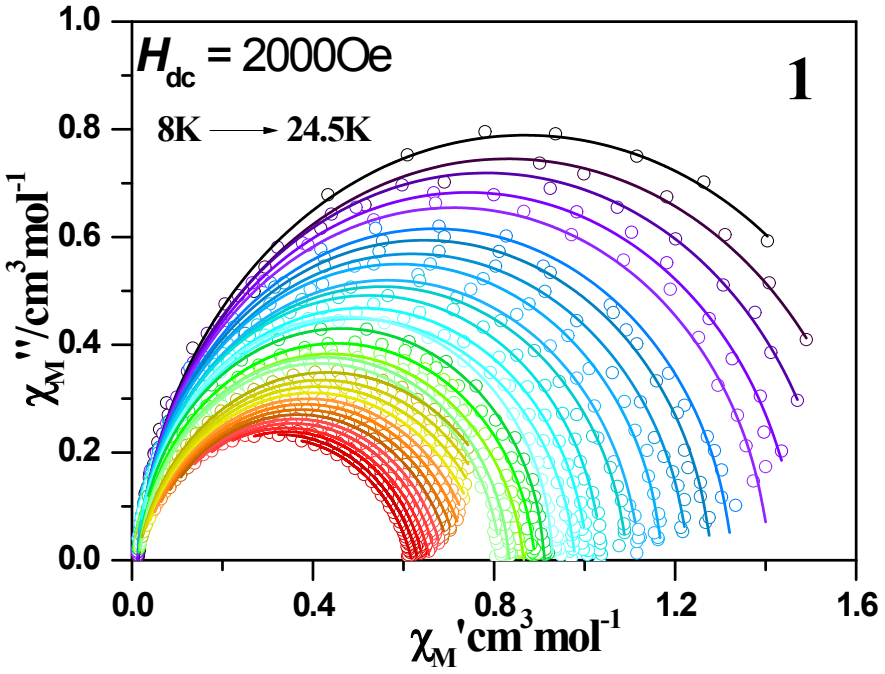

Fig. S12 Cole-cole plots of **1** under 2 kOe *dc* field.

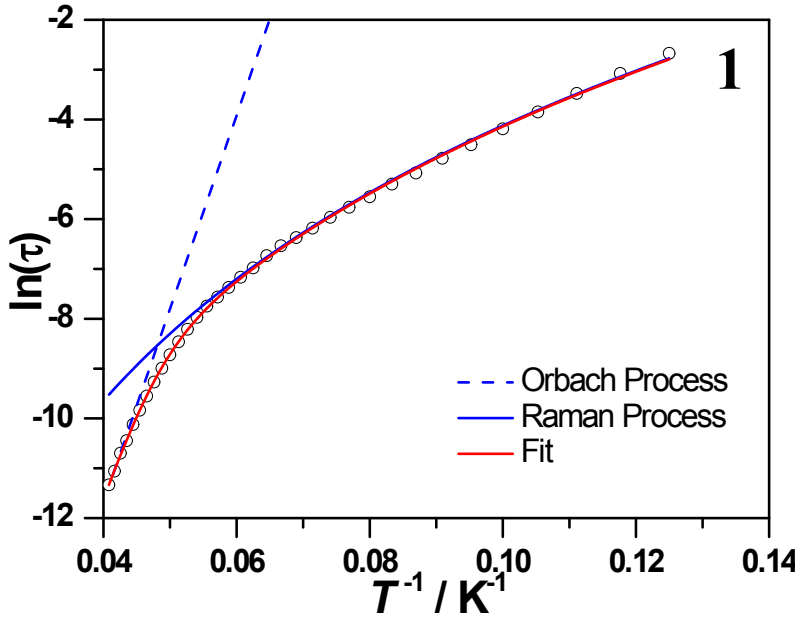

Fig. S13 Magnetic relaxation dynamics for **1** under 2 kOe *dc* field.

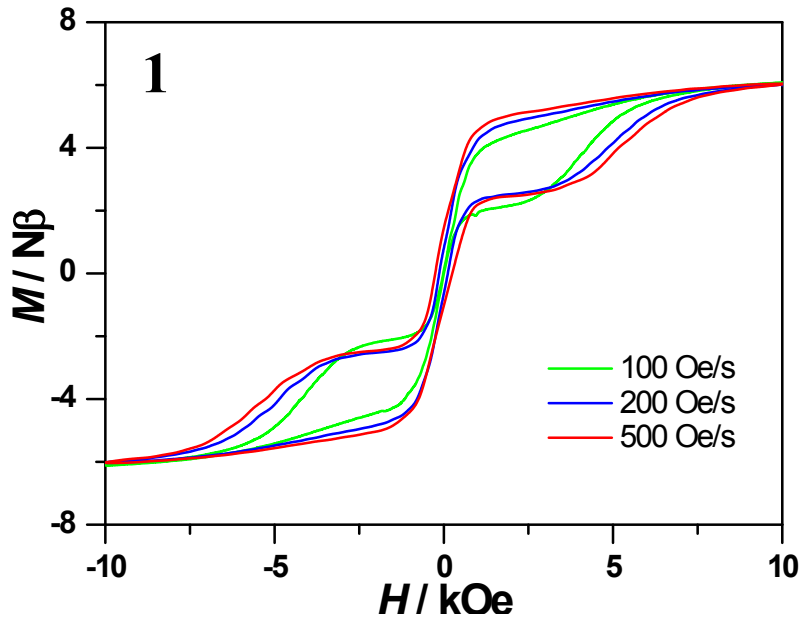

Fig. S14 Hysteresis loop for **1** measured with different sweep rates at 2 K.

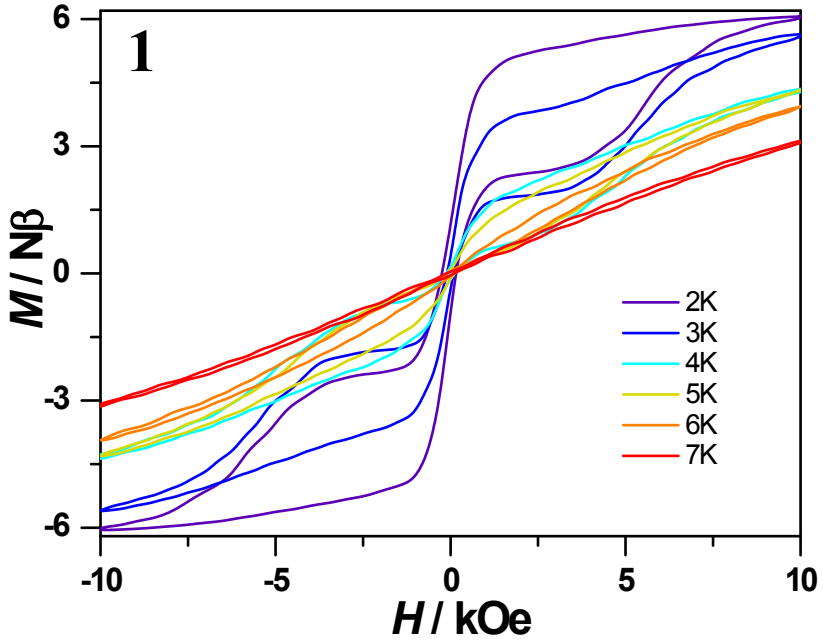

Fig. S15 Hysteresis loop for **1** measured at different temperatures with sweep rates of 500 Oe/s.

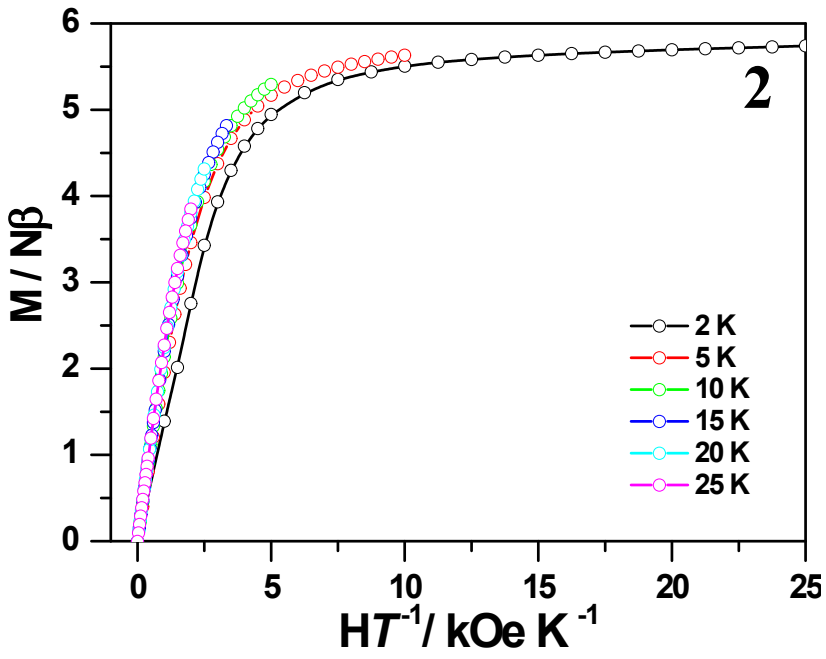

Fig. S16 Plots of *M*-*H* for **2**.

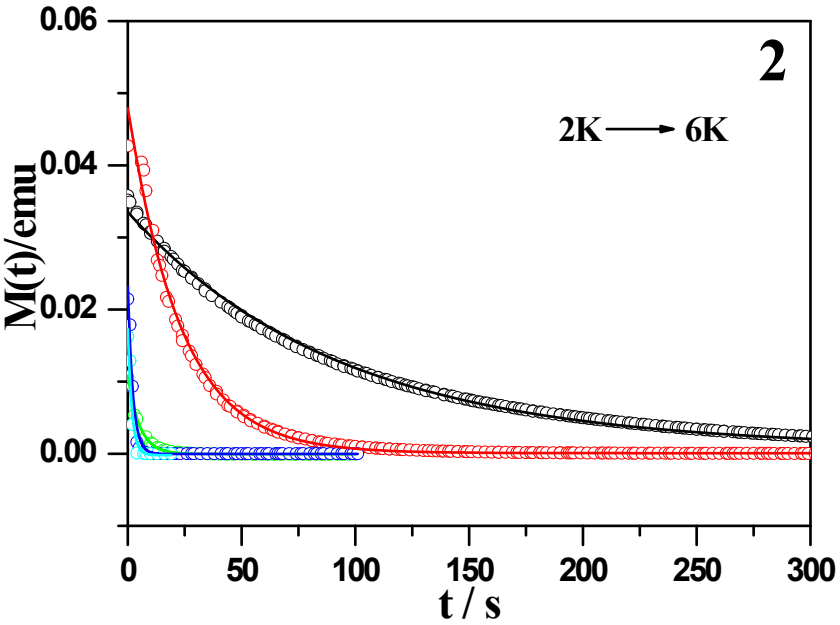

Fig. S17. DC relaxation of **2** with the final field of 0 Oe. The magnetizations are plotted as normalized to M_0 (the starting value at $t = 0$) for clarity. The solid lines are the best fit to the exponential decay as $M(t) = M_f + (M_f - M_0) \exp[(-t/\tau)^{\beta}]$, where τ is the relaxation time. Note the different scale of the time axis (x).

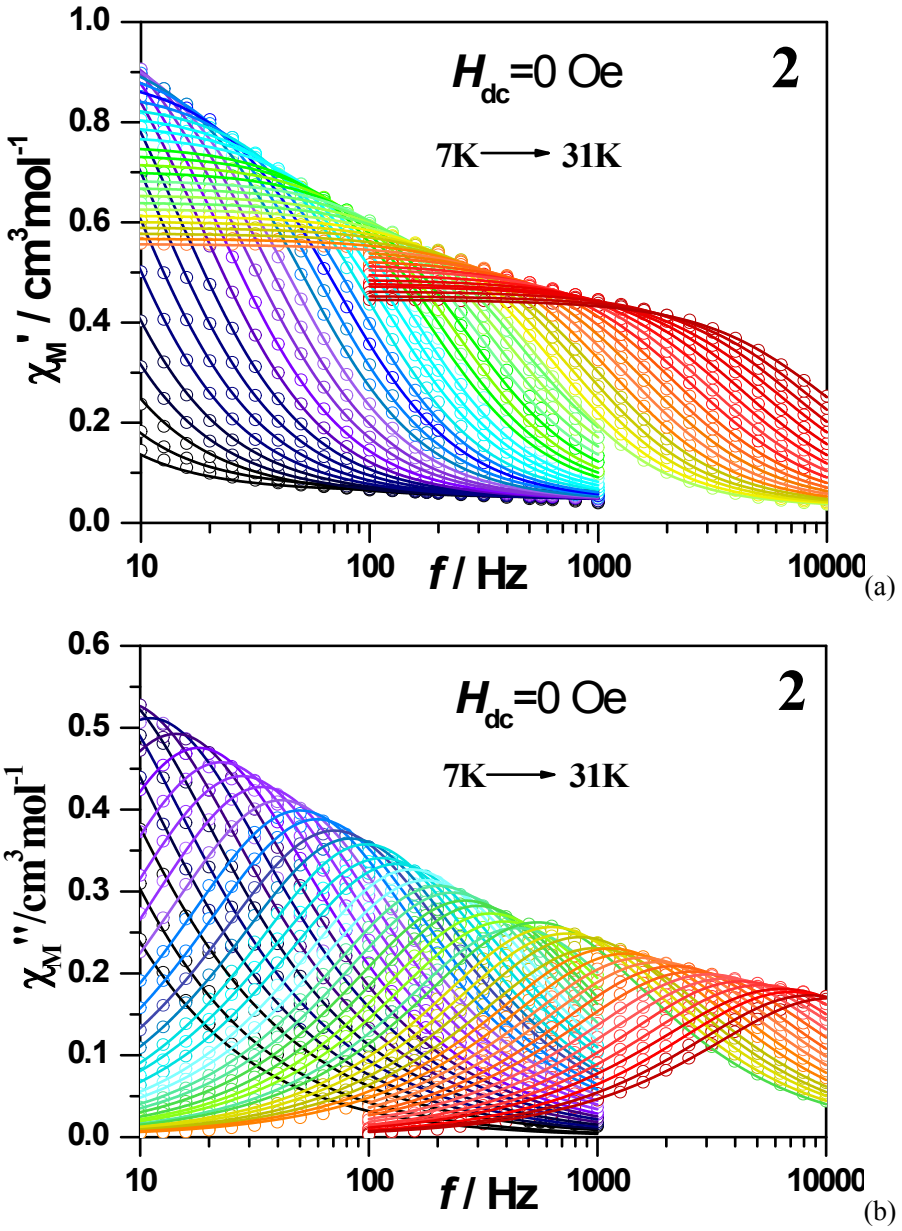

Fig. S18 *Ac-f* curves measured under zero *dc* fields for **2**. Solid lines were fitted using a generalized Debye relaxation model, simultaneously to χ'(*f*) and χ'' (*f*) curves.

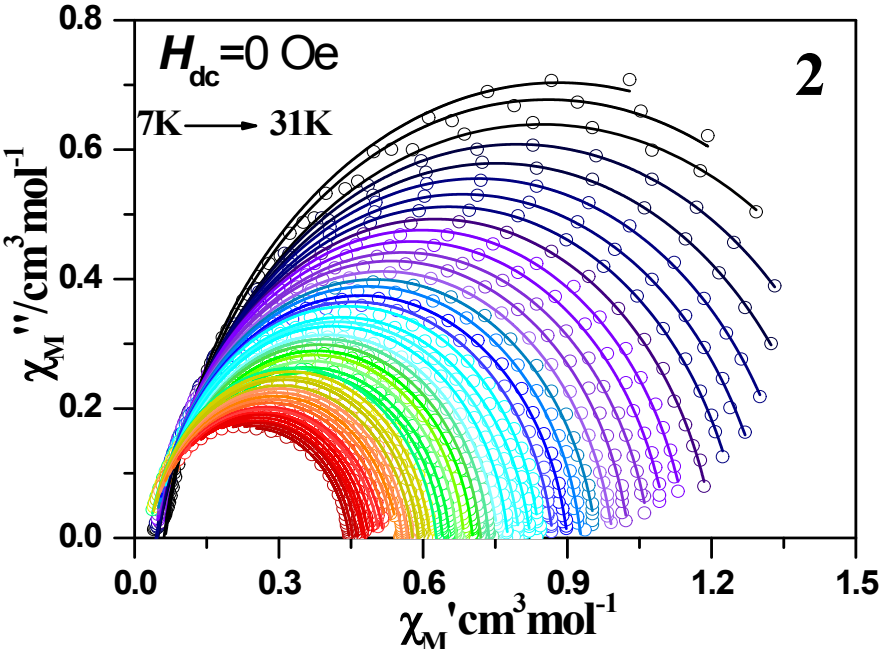

Fig. S19 Cole-cole plots of **2** under zero *dc* field.

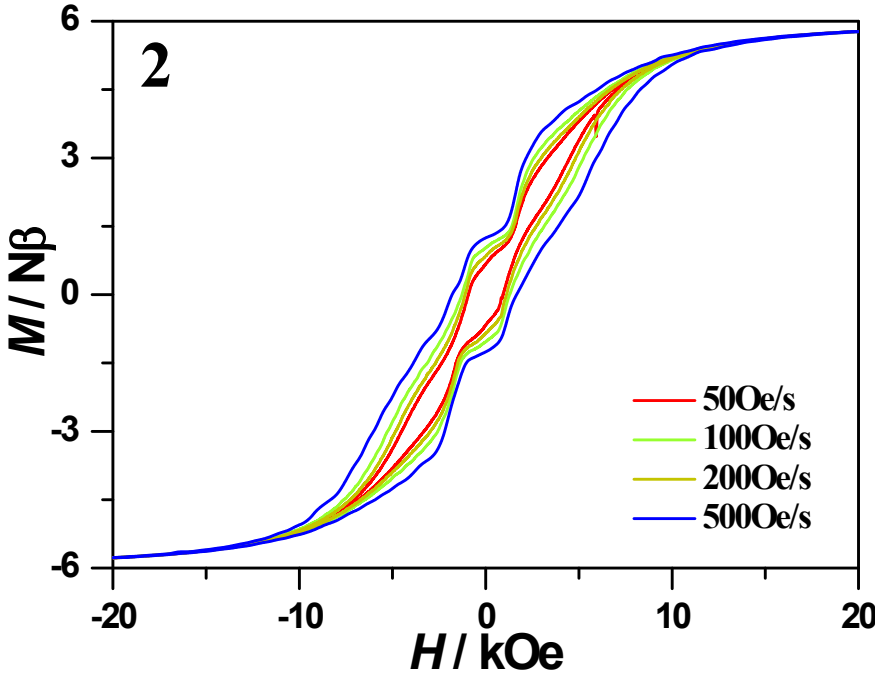

Fig. S20 Hysteresis loop for **2** measured with different sweep rates at 2 K.

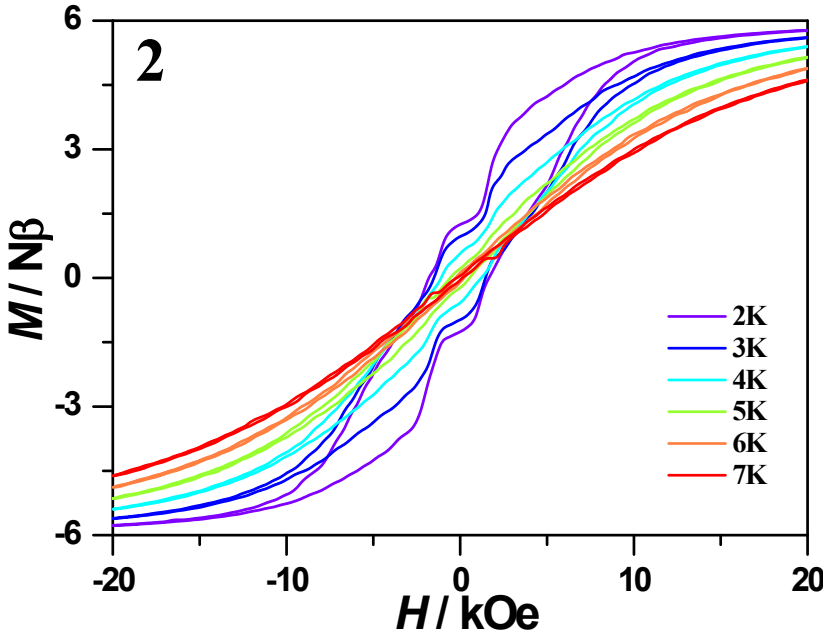

Fig. S21 Hysteresis loop for **2** measured at different temperatures with sweep rates of 500 Oe/s.

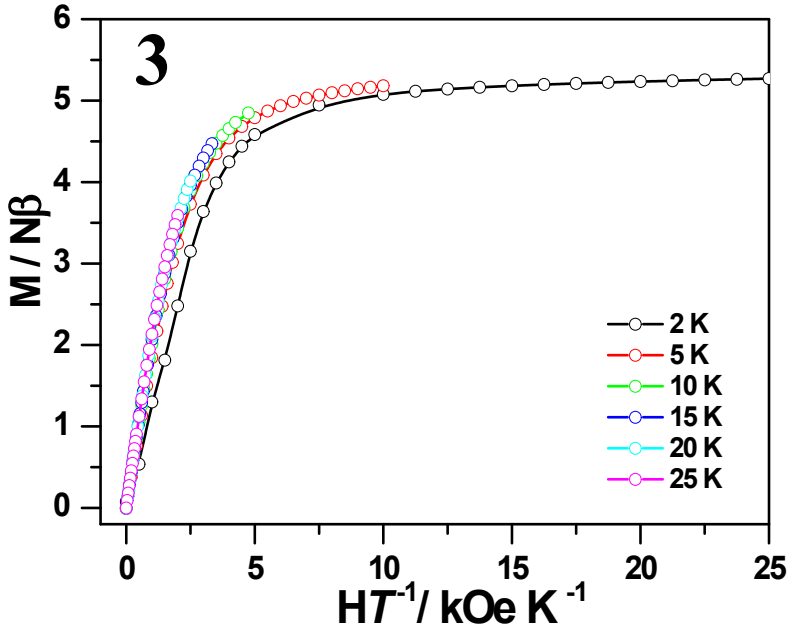

Fig. S22 Plots of *M*-*H* for **3**.

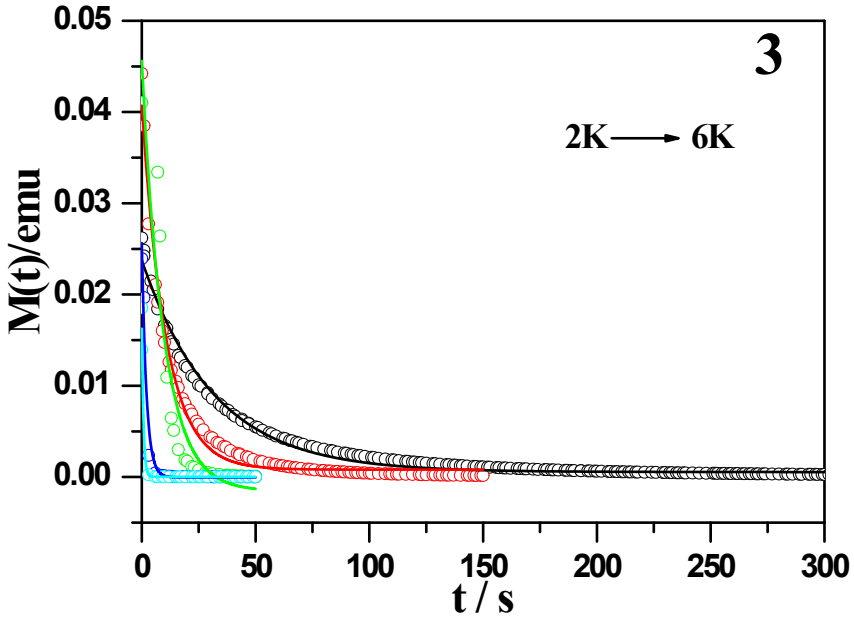

Fig. S23 DC relaxation of **3** with the final field of 0 Oe. The magnetizations are plotted as normalized to M_0 (the starting value at $t = 0$) for clarity. The solid lines are the best fit to the exponential decay as $M(t) = M_f + (M_f - M_0) \exp[(-t/\tau)^{\beta}]$, where τ is the relaxation time. Note the different scale of the time axis (x).

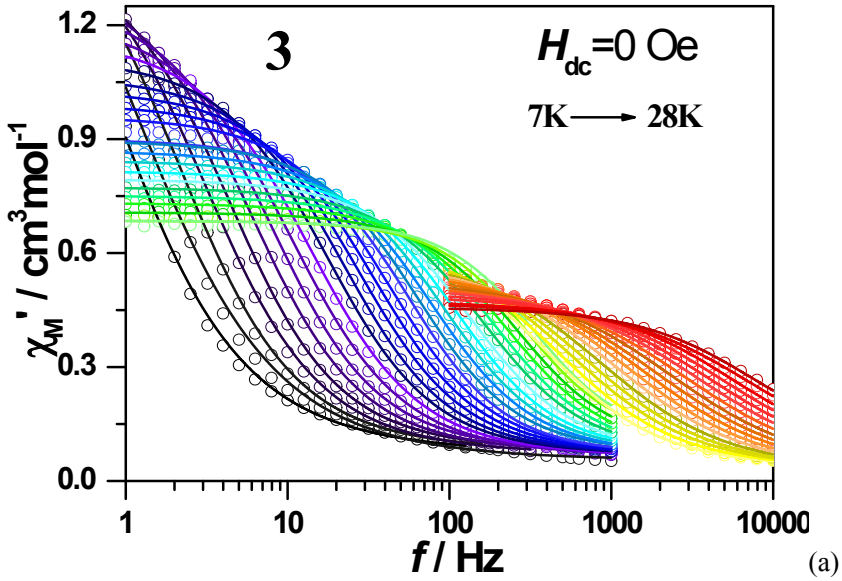

(a)

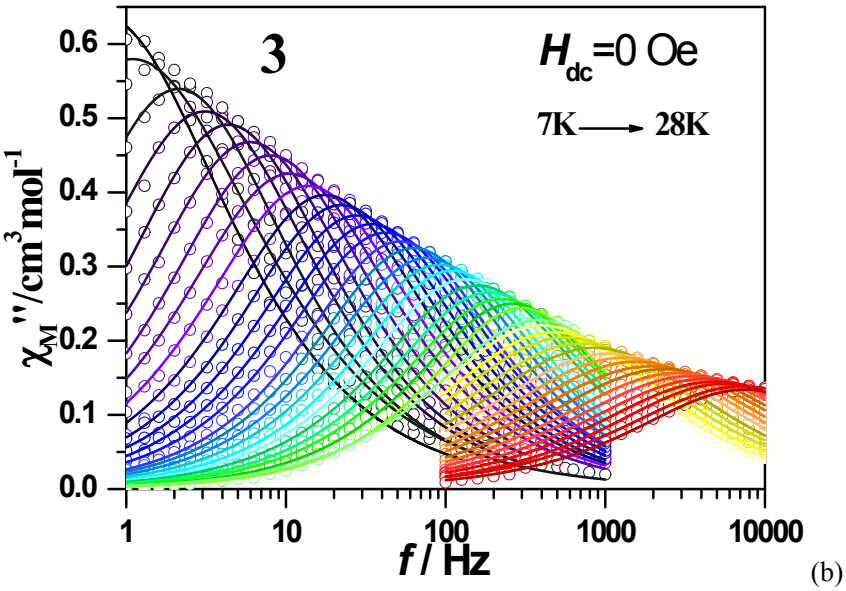

(b)

Fig. S24 *Ac-f* curves measured under zero *dc* fields for **3**. Solid lines were fitted using a generalized Debye relaxation model, simultaneously to χ'(*f*) and χ'' (*f*) curves.

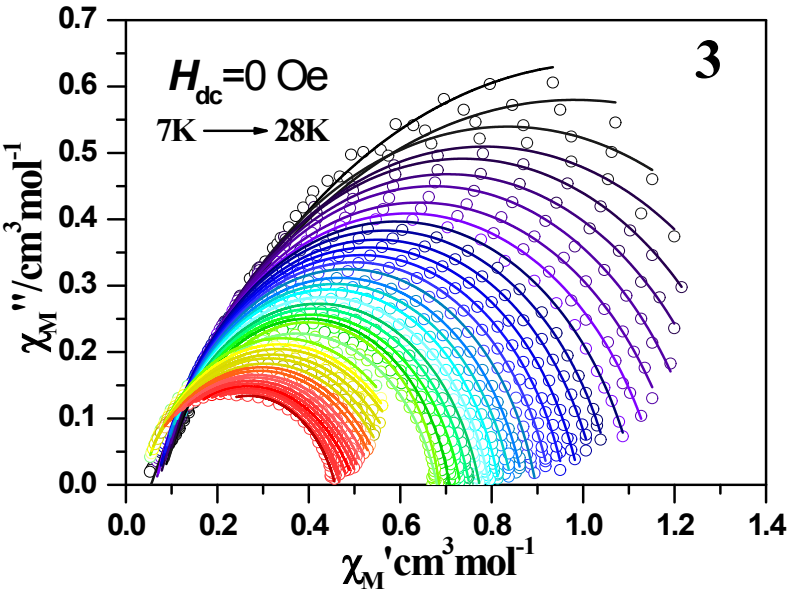

Fig. S25 Cole-cole plots of **3** under zero *dc* field.

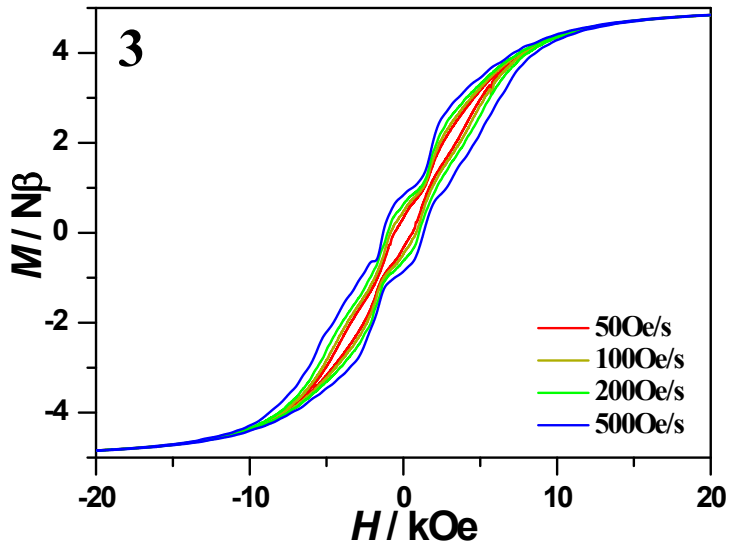

Fig. S26 Hysteresis loop for **3** measured with different sweep rates at 2 K.

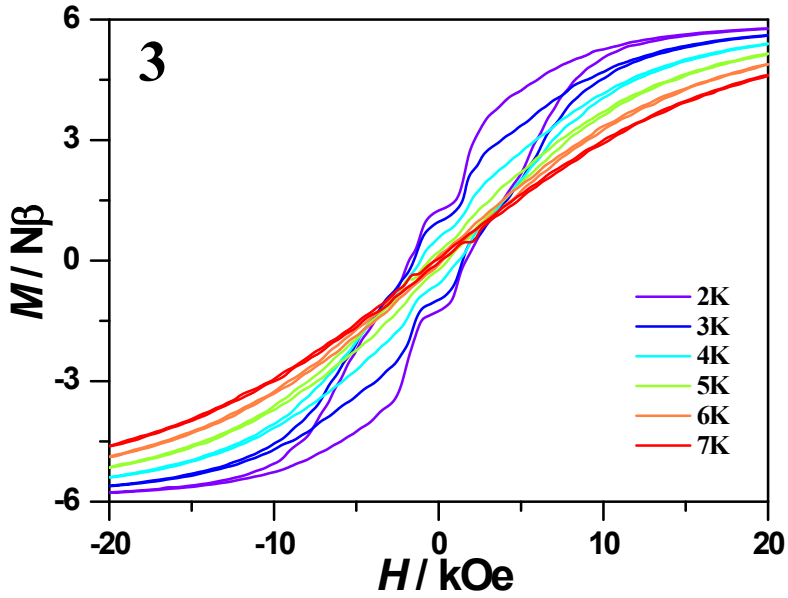

Fig. S27 Hysteresis loop for **3** measured at different temperatures with sweep rates of 500 Oe/s.

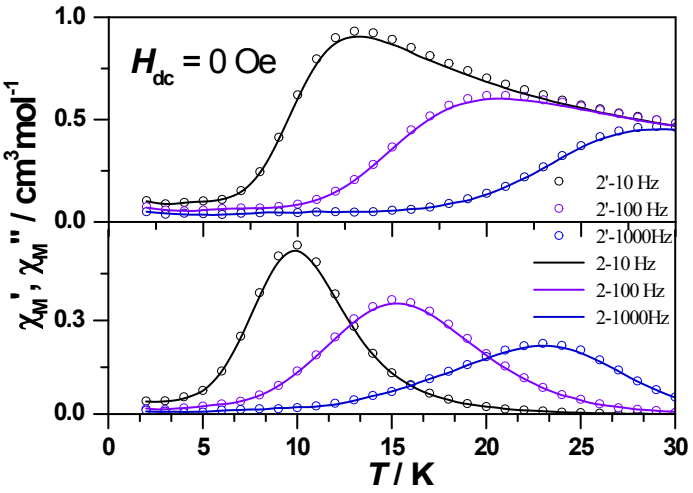

Fig. S28 Temperature dependence of the in-phase χ_M' (top) and out-of-phase χ_M'' (bottom) ac signals at 10Hz, 100 Hz and 1000 Hz under zero dc field for **2** and **2'**.

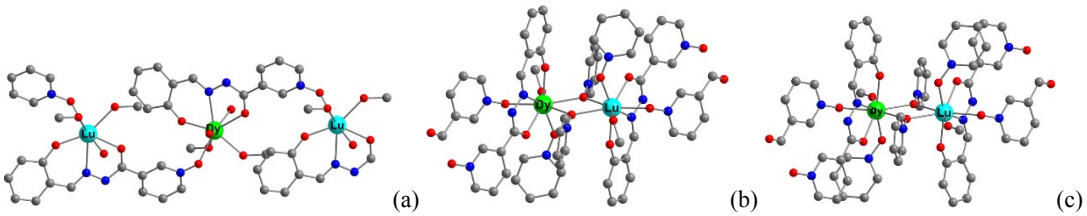

Fig. S29 Calculated model structure for complex complexes **1** (a), **2** (b) and **3** (c); H atoms are omitted.

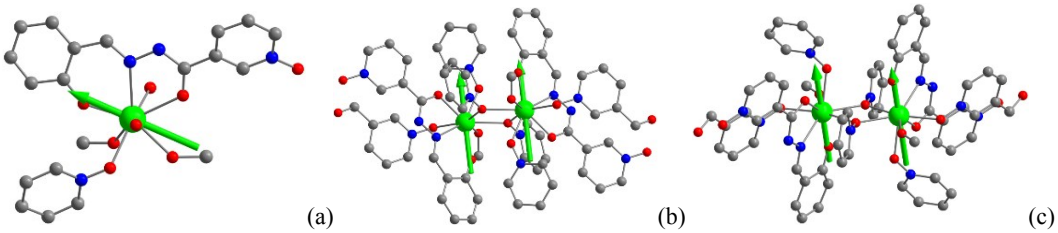

Fig. S30 Orientation of the local main magnetic axes of the ground Kramers doublet on Dy^{3+} ion of complexes **1** (a), **2** (b) and **3** (c).

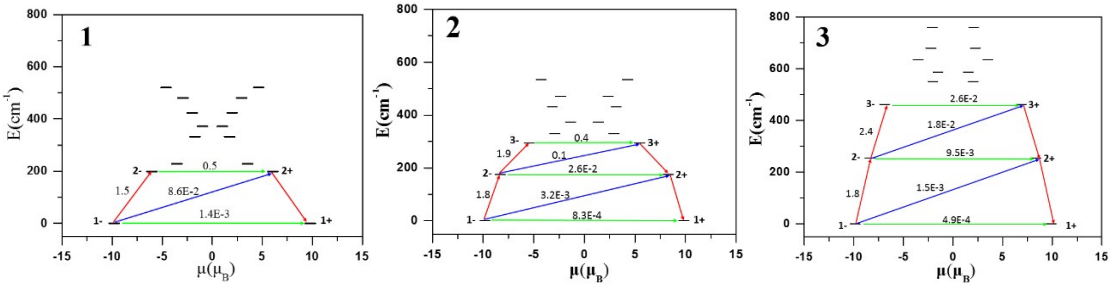

Fig. S31 The magnetization blocking barriers in complexes **1**-**3**. The thick black lines represent the Kramers doublets as a function of their magnetic moment along the magnetic axis. The green lines correspond to diagonal quantum tunneling of magnetization (QTM); the blue line represent off-diagonal relaxation process. The numbers at each arrow stand for the mean absolute value of the corresponding matrix element of transition magnetic moment.